Protrusion of nanospikes on cholesterol-containing microgels by reduction-responsive self-assembly in cell milieu and its influence on cell functions†

Zihe Zhai,‡[a] Wenbo Zhang,‡[a] Ning Ding,[a] Xue Lin[a] and Changyou Gao ⓘ *[ab]

Self-assembly in living systems is important for developing biological functional materials and regulating cellular processes, which have potential applications in disease diagnosis and treatment. However, the controllable fabrication of complex self-assemblies such as micro/nanocomposite structures and the direct observation of morphology-defined nanostructures in a cell milieu are still challenging. We report here a facile strategy for achieving the intracellular stimuli-responsive fabrication of micro/nanocomposite structures by using reduction-responsive microgels as a platform. Amphiphilic polymers (CSEG-*g*-Chol) that contained disulfide bonds in side chains and grafted cholesterol groups (Chol) were synthesized and used to prepare microgels (MGs) by a method based on a calcium carbonate template, in which the template was removed after the polymer was loaded and crosslinked. In the presence of reductants such as glutathione (GSH) and dithiothreitol (DTT), nanospikes gradually protruded from the surface of CSEG-*g*-Chol MGs. After internalization into cells, reduction-responsive self-assembly and the protrusion of nanospikes in the cell milieu were observed. No obvious influence on the cytoskeleton and endoplasmic reticulum was observed *via* light microscopy. However, co-incubation of the MGs caused a certain extent of cytotoxicity depending on the co-incubation concentration and stimulated the secretion of tumor necrosis factor-α (TNF-α), which was several times higher than in the control group. This work may serve as a paradigm for the study of intracellular and *in vivo* self-assembly and may also provide important insights for the investigation of biological self-assembly and interactions between micro/nanomaterials and cells.

Introduction

Nature can produce highly complex nanostructures *via* deliberately adjusted self-assembly. In biological systems, to a certain extent, most basic structures such as genes, enzymes, antibodies and viruses are formed by bottom-up self-assembly.[1] Inspired by nature, supramolecular self-assembly has been widely utilized for fabricating functional nano/microarchitectures.[2,3] In particular, stimuli-responsive self-assembly regulates the fabrication process in a controlled manner and is thereby very efficient for obtaining versatile organic nanomaterials.[4–6]

Besides the development of nanomaterials in solutions and the study of their interactions with biological systems,[7–9] self-assemblies in living systems have attracted increasing attention in recent years.[10–12] Intracellular or *in vivo* self-assembly represents an important system for developing biological functional materials and regulating cellular processes, which have potential applications in disease diagnosis and treatment. For instance, Xu *et al.* reported the detection of enzymatic activity by a self-assembled hydrogel inside living cells.[13] Recently, Wang *et al.* achieved the *in situ* formation of nanofibers of purpurin 18-peptide conjugates, which exhibited an assembly-induced retention effect at tumor sites.[14] Nonetheless, the direct observation of morphology-defined nanostructures has rarely been reported, especially in the cases of organic and polymeric materials, owing to low contrast in a cell milieu. The controllable fabrication of complex self-assemblies such as micro/nanocomposite structures in a cell milieu is even more challenging.
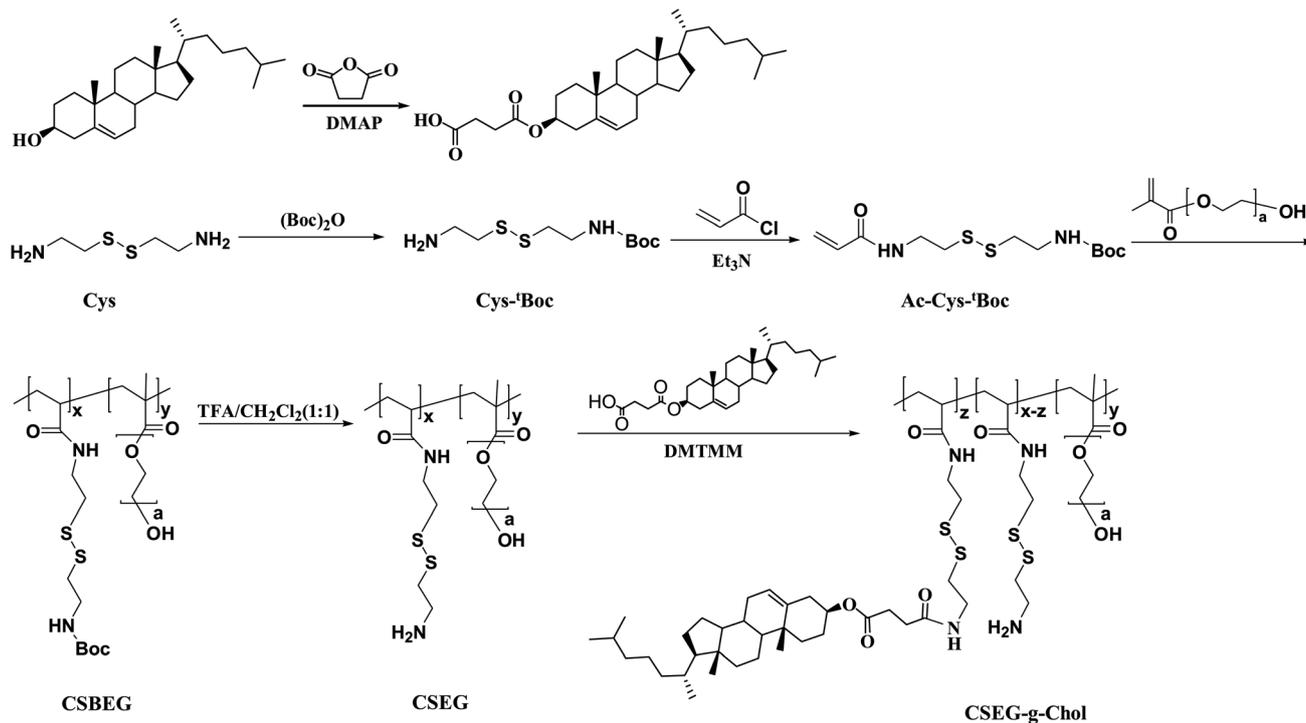
Here, we propose a facile strategy for achieving the intracellular stimuli-responsive fabrication of micro/nanocomposite structures by using reduction-responsive microgels (MGs)

[a] MOE Key Laboratory of Macromolecular Synthesis and Functionalization, Department of Polymer Science and Engineering, Zhejiang University, Hangzhou 310027, China. E-mail: cygao@zju.edu.cn
[b] Dr. Li Dak Sum & Yip Yio Chin Center for Stem Cell and Regenerative Medicine, Zhejiang University, Hangzhou 310058, China
† Electronic supplementary information (ESI) available. See DOI: 10.1039/c8qm00345a
‡ Z. H. Zhai and W. B. Zhang contributed equally to this work.

This journal is © The Royal Society of Chemistry and the Chinese Chemical Society 2019

Mater. Chem. Front., 2019, **3**, 233–241 | 233

Scheme 1   Synthesis scheme of the cholesterol-containing amphiphilic copolymer CSEG-*g*-Chol.

as a platform. We rationally designed an amphiphilic polymer (CSEG-*g*-Chol) that contained disulfide bonds and grafted cholesterol groups (Chol) in side chains (Scheme 1). Then, polymeric replica microgels were prepared by a method based on a porous $CaCO_3$ template, in which the template was removed after the polymer was loaded and crosslinked. Cholesterol, which is ubiquitous both on the cell surface and inside cells, was chosen as the main self-assembly building block for the following reasons. Cholesterol has been utilized as a building block to form various nanostructures by self-assembly.[15–17] In addition, the interactions

between proteins and cholesterol are critical for cellular functions[18,19] and may be used for regulating cell processes. The CSEG-*g*-Chol MGs that were obtained underwent a reduction-responsive shape transformation in the presence of reductants such as glutathione (GSH) and dithiothreitol (DTT), which led to the gradual protrusion of nanospikes from their surface. After being internalized into cells, the MGs underwent reduction-responsive self-assembly to form nanospikes on their surface in a cell milieu containing GSH (Scheme 2). This work demonstrates for the first time that morphology-defined micro/nanocomposite
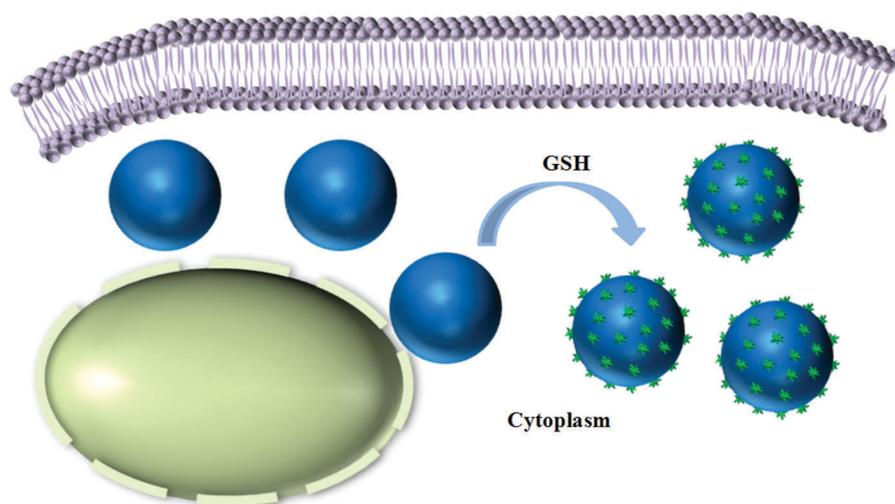
Scheme 2   Schematic illustration showing the intracellular reduction-responsive formation of micro/nanocomposite particles in the presence of glutathione (GSH).

structures can be obtained *via* intracellular stimuli-responsive self-assembly. Moreover, self-assembled nanospikes were easily observed in cells by using the CSEG-*g*-Chol MGs as a platform, which has hitherto been a challenging task. On this basis, the interactions between the MGs and cells and the influence of the intracellular reduction-responsive decomposition-assembly of the CSEG-*g*-Chol MGs on cell functions were studied, which may provide important insights for the investigation of interactions between micro/nanomaterials and cells.

Results and discussion

Cholesterol derivatives were chosen in this study owing to their extensive use as self-assembly units to form various nano-structures[20,21] and good performance in biological applications (*e.g.*, cancer therapy).[19,22] The cholesterol derivative cholesterol-3-hemisuccinate ester (Chol-COOH) was synthesized by the reaction between cholesterol and succinic anhydride, which afforded cholesterol with a carboxylic functionality[23,24] (Scheme 1 and ESI,† Fig. S1).

The disulfide-bond-containing monomer *N-tert*-butoxycarbonyl-*N'*-acryloylcystamine (Ac-Cys-^{t}Boc) was synthesized from cystamine in two steps. Firstly, one amino group of cystamine (Cys) was protected with a *tert*-butoxycarbonyl group (^{t}Boc) to obtain the intermediate Cys-^{t}Boc, and then the other amino group of Cys-^{t}Boc reacted with acryloyl chloride to yield the monomer Ac-Cys-^{t}Boc (Scheme 1 and ESI,† Fig. S2, S3). The reduction-responsive copolymer CSEG was synthesized by free-radical polymerization of Ac-Cys-^{t}Boc and poly(ethylene glycol) methacrylate (PEGMA), and its structure was characterized and confirmed by ^{1}H NMR and gel permeation chromatography (GPC) (ESI,† Fig. S4 and S5). A copolymer with a molecular weight of 3.5 kDa (M_n, GPC) and a structural unit ratio of 2.7 : 1 ([Ac-Cys-^{t}Boc] : [PEGMA]) was chosen in the following studies. After deprotection, the polymer was conjugated with hydrophobic Chol groups to obtain the amphi-philic polymer CSEG-*g*-Chol. The ^{1}H NMR spectrum (ESI,† Fig. S6) displays the signals of both Chol and CSEG, which suggests the successful grafting of Chol. The structural unit ratio ([Ac-Cys-Chol] : [Ac-Cys] : [PEGMA]) in CSEG-*g*-Chol was calculated to be 1.3 : 1.4 : 1.

To prepare the CSEG-*g*-Chol MGs, porous CaCO₃ micro-particles (1.76 ± 0.31 μm) were synthesized and used as a template. To facilitate the efficient loading of CSEG-*g*-Chol, a vacuum was applied to the suspension, which enabled the infiltration of the polymer into nanopores in the template. The electrostatic interactions between CSEG-*g*-Chol and CaCO₃ could also play a role in loading. After the amine groups were crosslinked with glutaraldehyde (GA) and the template was removed, CSEG-*g*-Chol MGs were obtained (Scheme 2). To promote cellular uptake and improve their dispersion in an aqueous solution, the MGs were further modified with Tat peptide by the Schiff base reaction between residual aldehyde groups in the MGs and amino groups in Tat peptide. As shown in Fig. 1, the CSEG-*g*-Chol MGs that were obtained were intact with an average size of 1.55 ± 0.25 μm (Fig. 1a) and had a solid interior (Fig. 1b) and a
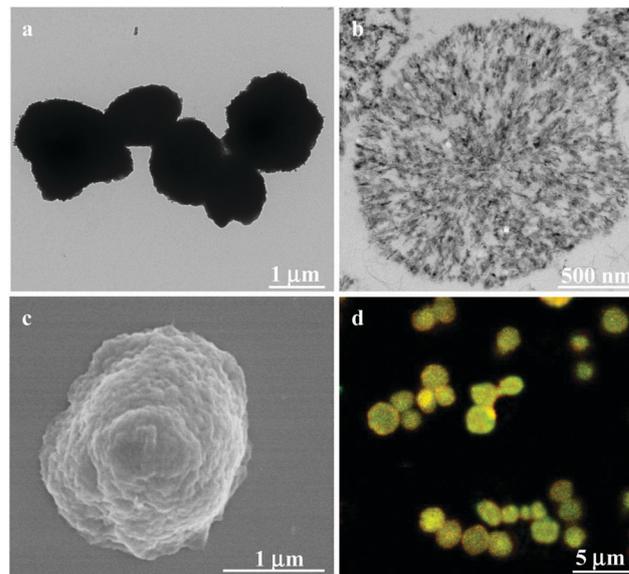

Fig. 1 (a) TEM, (b) cross-sectional (ultramicrotomy) TEM, (c) SEM and (d) CLSM images of CSEG-*g*-Chol microgels (MGs). The yellow fluorescence is the combined effect of the green and red autofluorescence.

rugged surface (Fig. 1c). They were well dispersed in water and exhibited bright and stable autofluorescence without deliberate conjugation to any fluorophore (ESI,† Fig. S7a–c). The fluores-cence is ascribed to the n–π* transition of the C=N bonds in the Schiff base that was formed.[25,26] These properties are favorable for fluorescence imaging and potential applications in biological fields.

The presence of reduction-responsive disulfide bonds provides convenient trigger sites for the controllable self-assembly and shape evolution of well-defined supramolecular entities. It has been reported that cholesterol derivatives can form various kinds of self-assemblies, such as nanorods and nanovesicles. The progressive protrusion and growth of nanospikes on the surface of the CSEG-*g*-Chol MGs was observed when the MGs were incubated in a GSH solution (5 mM) at 37 °C (Fig. 2a–f). As shown in the TEM images, after 0.5 h the contrast at the periphery of the MGs faded, which was accompanied by the appearance of small nanospikes and nanoaggregates (several tens of nanometers) on the surface of the MGs, as well as around the MGs (Fig. 2b). The size of the nanospikes increased as the incubation time was prolonged (Fig. 2c and d) and reached several hundred nano-meters at 3 h (Fig. 2d). Incubation for an even longer time resulted in further fading of the contrast around the MGs in parallel with the smoothing of the nanospikes (Fig. 2e and f).

The formation of the nanospikes on the surface of the CSEG-*g*-Chol MGs should be related to changes in the chemical structure caused by the reduction-responsive cleavage of the disulfide bonds and the self-assembly of the released Chol groups. In order to prove this hypothesis, we synthesized the monomer Ac-DAH-^{t}Boc (ESI,† Scheme S1 and Fig. S8, S9) and the amphiphilic polymer ADEG-*g*-Chol (ESI,† Scheme S1 and Fig. S10–S12), which have analogous chemical structures to Ac-Cys-^{t}Boc and CSEG-*g*-Chol, respectively. ADEG-*g*-Chol microgels
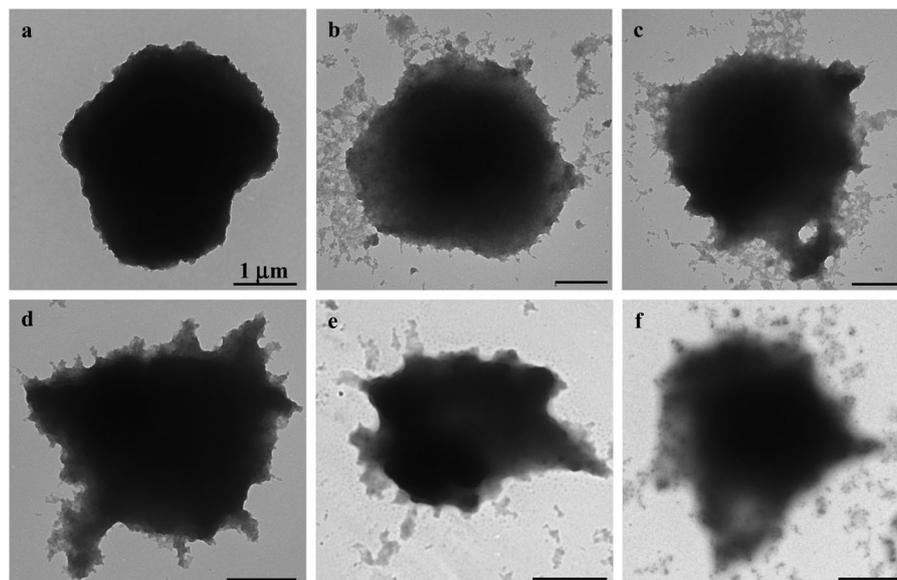
This journal is © The Royal Society of Chemistry and the Chinese Chemical Society 2019

Mater. Chem. Front., 2019, **3**, 233–241 | **235**

Fig. 2 TEM images showing the process of the protrusion of nanospikes on the surface of CSEG-*g*-Chol MGs after being incubated in a glutathione solution (5 mM) for 0 (a), 0.5 (b), 1 (c), 3 (d), 12 (e) and 24 h (f), respectively.

were prepared by the same templating-crosslinking method and owing to their structures were not reduction-responsive. CLSM characterization showed that the ADEG-*g*-Chol MGs that were obtained had similar sizes and autofluorescence properties (ESI,† Fig. S13a–c). However, after being incubated in a GSH solution (5 mM, 37 °C) for 0.5 h to 24 h, the morphology of the ADEG-*g*-Chol MGs exhibited no obvious change (ESI,† Fig. S14a–d). These results demonstrate that under the influence of GSH the reduction-responsive cleavage of disulfide bonds in the CSEG-*g*-Chol MGs induced the self-assembly of released Chol
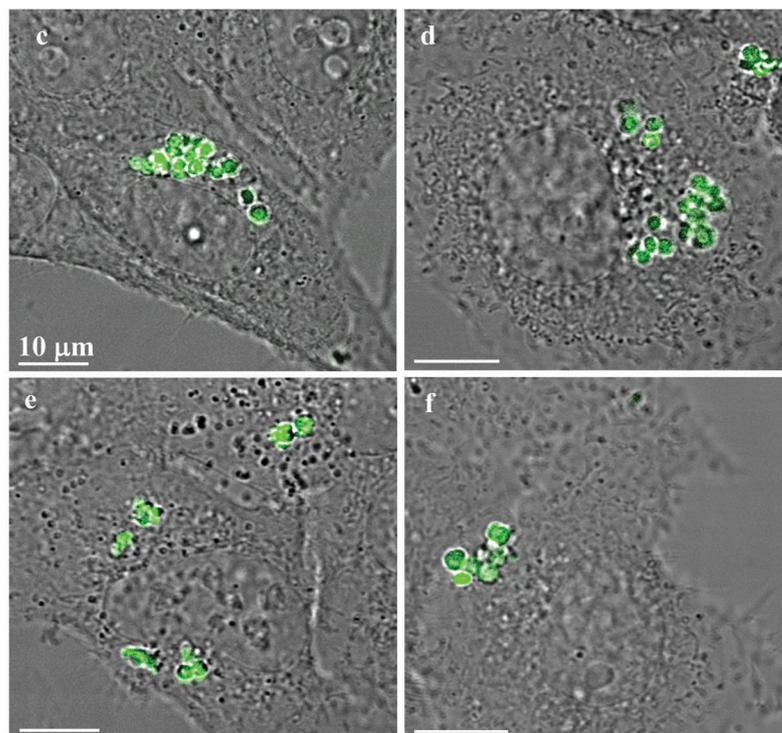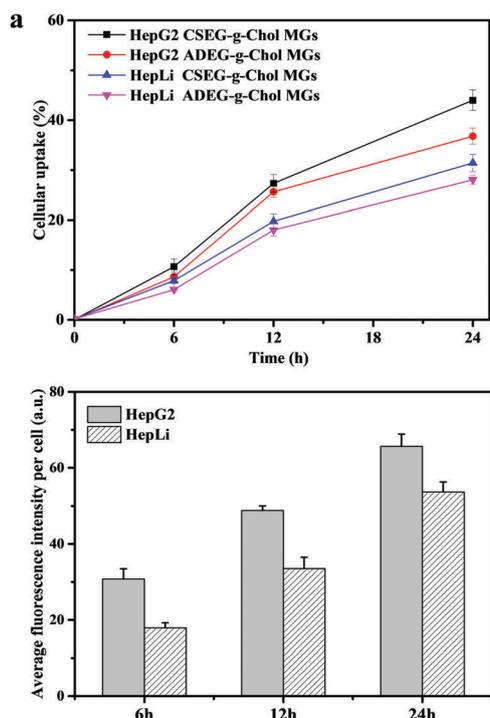

Fig. 3 Characterization of cellular uptake of CSEG-*g*-Chol and ADEG-*g*-Chol MGs. Flow cytometry results showing the ratios of cells that internalized MGs as a function of the incubation time (a) and the cellular uptake amounts of CSEG-*g*-Chol MGs (b) after co-incubation for a designated time at a particle : cell ratio of 15 : 1. CLSM images showing the uptake performance of CSEG-*g*-Chol MGs (c and d) and ADEG-*g*-Chol MGs (e and f) after being incubated with HepG2 (c and e) and HepLi (d and f) cells at a particle : cell ratio of 15 : 1 for 24 h. Data are expressed as the mean ± SD, $n = 3$, *$p < 0.05$, **$p < 0.01$.

This journal is © The Royal Society of Chemistry and the Chinese Chemical Society 2019

groups with those grafted on the polymer, which led to the formation of nanospikes. In the self-assembly process, the hydrophobic interactions between Chol groups, as well as hydrogen bonding between oxygen/nitrogen atoms and amino/hydroxyl groups, are believed to play an important role.[27,28] To demonstrate the generality of this reduction-responsive decomposition-assembly phenomenon, the MGs were also incubated in a dithiothreitol (DTT, 5 mM) solution at 37 °C. TEM monitoring demonstrated a similar phenomenon to that in the GSH solution. Nanospikes gradually protruded from the surface of the CSEG-g-Chol MGs with an increase in the incubation time (ESI,† Fig. S15a–c). In contrast, the ADEG-g-Chol MGs remained unchanged (ESI,† Fig. S15d–f). Hence, micro/nanocomposite structures can generally be formed by the reduction-triggered shape evolution of CSEG-g-Chol MGs.

Moreover, the surface chemical compositions of the microgels before and after reduction were analyzed by X-ray photoelectron spectroscopy (XPS). The surface C/O ratio and S content increased after the CSEG-g-Chol MGs were reduced (ESI,† Table S1), which suggests that more Chol groups (which had a higher carbon content, and each contained an –SH group) were present on the surface. In contrast, there were no obvious changes in either the surface C/O ratio or the S content of the ADEG-g-Chol MGs after treatment with GSH, which was consistent with the stability of their structure in reductive conditions. Polarizing microscopy revealed a birefringence phenomenon only in the CSEG-g-Chol micro/nanocomposite structures (ESI,† Fig. S16). These results reveal the formation of

anisotropic crystals,[29–31] which were formed by the self-assembly of released cholesterol groups.

Before their intracellular self-assembly was studied, the cellular uptake behavior of the MGs was investigated. Two human cell lines, namely, human liver hepatocellular carcinoma cells (HepG2) and normal primary human hepatocytes (HepLi), were chosen for the following investigations. Quantitative analysis of the cellular uptake of CSEG-g-Chol MGs and ADEG-g-Chol MGs was performed by flow cytometry. As shown in Fig. 3a, the internalization of both MGs was a time-dependent process in both kinds of cells. At 6 h, the proportions of cells that had internalized MGs were rather low. As the time was prolonged, the cellular uptake ratio increased gradually. After 24 h, about 44% and 37% of HepG2 cells had internalized CSEG-g-Chol MGs and ADEG-g-Chol MGs, respectively. The uptake ratios of CSEG-g-Chol MGs and ADEG-g-Chol MGs in the case of HepLi cells were both lower than those in the case of HepG2 cells at the same incubation time and reached 32% and 28%, respectively, after incubation for 24 h. Moreover, the cellular uptake numbers of CSEG-g-Chol MGs (Fig. 3b) and ADEG-g-Chol MGs (ESI,† Fig. S17) exhibited an increasing tendency similar to that of the cellular uptake ratios with an increase in the incubation time. The average number of internalized MGs in each HepG2 cell was slightly larger than that in each HepLi cell at the same incubation time. CLSM observations revealed that after co-incubation for 24 h the internalized MGs were mainly distributed in the cytoplasm and partly around the nuclei (Fig. 3c–f). None of the MGs could penetrate into the cell
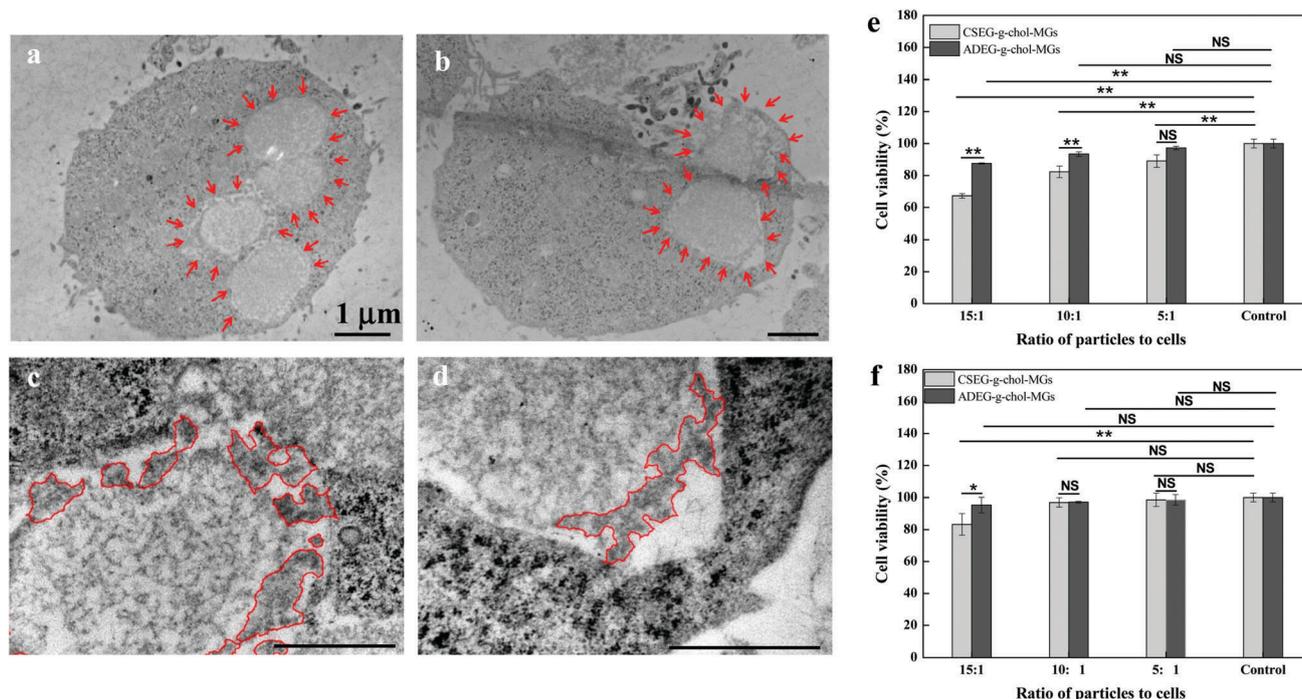

Fig. 4 Cross-sectional (ultramicrotomy) TEM images showing protruding nanospikes on the surface of CSEG-g-Chol MGs after the MGs were co-incubated with HepG2 (a and c) and HepLi (b and d) cells for 24 h at a particle : cell ratio of 15 : 1. The MGs are outlined by inward-pointing arrows (a and b), and the producing nanostructures are encircled by lines (c and d). Cytotoxicity of CSEG-g-Chol MGs after co-incubation with HepG2 (e) and HepLi (f) cells at particle : cell ratios of 15 : 1, 10 : 1 and 5 : 1, respectively, for 24 h. Data are expressed as the mean ± SD, n = 5, *p < 0.05, **p < 0.01. NS indicates no significant difference at a level of p < 0.05.

This journal is © The Royal Society of Chemistry and the Chinese Chemical Society 2019

Mater. Chem. Front., 2019, **3**, 233–241 | **237**

nuclei because their sizes were much larger than those of the nucleopores (the diameters of cylinder-like nucleopores are 25–30 nm).[32]

On the basis of the cellular uptake results, we co-incubated CSEG-*g*-Chol MGs with HepG2 and HepLi cells, respectively, for 24 h to investigate their intracellular reduction-responsive decomposition-assembly. As shown by TEM images (Fig. 4a and b), MGs were clearly observed inside the cytoplasm, which again confirmed their internalization. Because the thickness of the ultramicrotomed samples (100–300 nm) was much less than that of the CLSM imaging plane (1–2 μm), a smaller number of MGs were observed by TEM. The internalized MGs robustly maintained their original shape without obvious deformation. The reductant GSH is ubiquitous and is the most abundant (1–10 mM) thiolated tripeptide found within the human cellular system.[33,34] It has been widely utilized in interactions with reduction-responsive systems in drug delivery and cell imaging. Taking into account the advantage of its relatively large size in comparison with the structures and molecules in cells, it is convenient for directly observing the intracellular stimuli-responsive self-assembly of reduction-responsive MGs. In higher-magnification TEM images, the protrusion of nanospikes from the surface of CSEG-*g*-Chol MGs was successfully observed in both HepG2 (Fig. 4c) and HepLi (Fig. 4d) cells. In contrast, no apparent nanospikes were found on the periphery of the unresponsive ADEG-*g*-Chol MGs in either kind of cell under the same conditions (ESI,† Fig. S18).

Therefore, we can safely conclude that the CSEG-*g*-Chol MGs underwent reduction-responsive decomposition-assembly in the cell milieu to form the novel microgel/nanospikes composite structures *in situ*. As far as we know, the formation of well-defined self-assembled nano/microstructures in a cell milieu has rarely been observed, especially that of novel micro/ nanocomposite structures.

To gain more insight into the interactions between the MGs and cells, as well as the influence of the intracellular reduction-responsive decomposition-assembly of the CSEG-*g*-Chol MGs on cells, the cytotoxicity of the MGs was measured by a standard MTT assay and the effects of the MGs on the cytoskeleton and endoplasmic reticulum of cells were analyzed *via* light microscopy. The MTT results show that after co-incubation of CSEG-*g*-Chol MGs with HepG2 cells for 24 h the cytoviability was affected to some extent, in particular at higher ratios of particles to cells (Fig. 4e). For example, only 67% of the viability of HepG2 cells was maintained when the particle : cell ratio was 15 : 1. ADEG-*g*-Chol MGs exhibited less influence on the cytoviability under the same conditions. For example, the viability of HepG2 cells was still as high as 88% when the particle : cell ratio was 15 : 1 (Fig. 4e). Considering the cellular uptake results, *i.e.*, the average number of internalized CSEG-*g*-Chol MGs in each HepG2 cell (Fig. 3b) was about 1.2 times that of ADEG-*g*-Chol MGs (ESI,† Fig. S17), it can be inferred that the higher cytotoxicity of the CSEG-*g*-Chol MGs was mainly due to the higher cellular uptake number. When CSEG-*g*-Chol MGs were co-incubated with HepLi cells at a
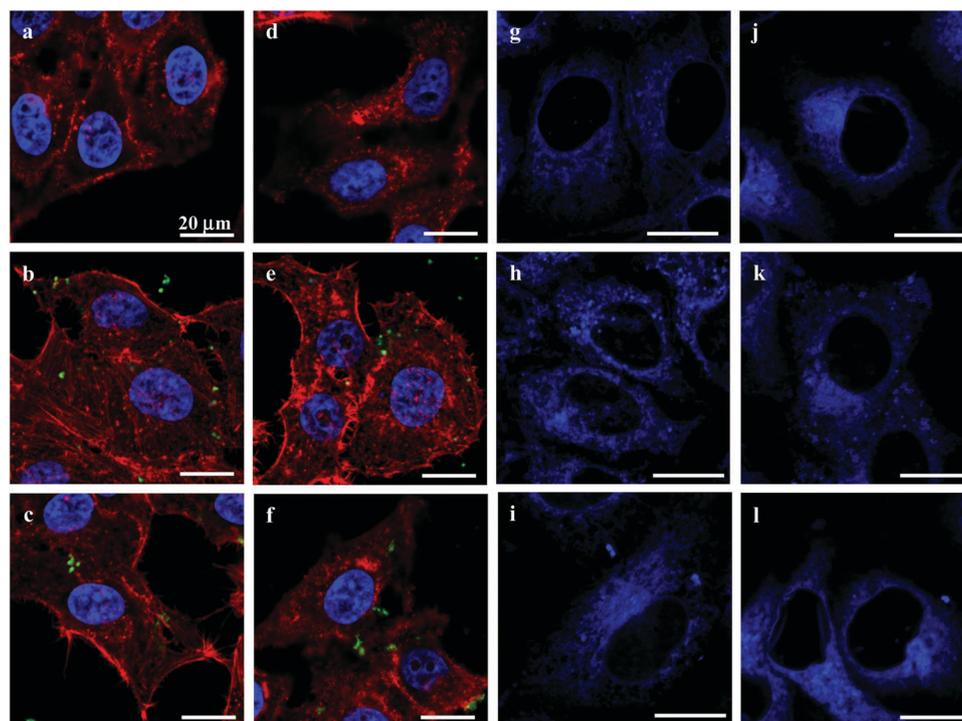

Fig. 5 CLSM images showing the cytoskeleton (red) and cell nuclei (blue) (a–f) and endoplasmic reticulum (g–l) of HepG2 (a–c and g–i) and HepLi (d–f and j–l) cells either untreated (a, d, g, j) or treated with CSEG-*g*-Chol MGs (b, e, h, k, green) or ADEG-*g*-Chol MGs (c, f, i, l, green) at a particle : cell ratio of 15 : 1 for 24 h. F-Actin was stained with rhodamine-conjugated phalloidin, the cell nuclei were stained with DAPI and the endoplasmic reticulum was stained with ER-Tracker Blue-White DPX.

particle : cell ratio of 15 : 1, the cell viability was still greater than 83% (Fig. 4f). This result is consistent with the lower cellular uptake number in comparison with that in the case of HepG2 cells. From these results, we can conclude that the intracellular reduction-responsive decomposition-assembly of CSEG-*g*-Chol MGs had no apparent influence on cell viability in comparison with the unresponsive ADEG-*g*-Chol MGs. We found previously that the intracellular stimuli-responsive shape transformation of pH-labile and photolabile pyrene-containing micelles resulted in significant cytotoxicity.[35,36] In contrast, the low cytotoxicity in the case of the transformation of CSEG-*g*-Chol MGs into micro/nanocomposite structures was probably due to the high cytocompatibility of the cholesterol group and the relatively slight changes in shape in comparison with their original shape.

The cytoskeleton of cells plays important roles in controlling the cell morphology and intracellular transport, as well as cell adhesion, migration, and division.[37] The endoplasmic reticulum (ER) performs many functions, such as the folding of protein molecules, the transport of synthesized proteins, the correct folding of newly made proteins and the biosynthesis of lipids.[38] The proper functioning of the ER is essential to cell survival, and perturbations of its functions induce cellular damage and result in apoptosis.[39] To study the effects of the MGs on the cytoskeleton

and ER, actin fibers (microfilaments) and ER were stained with rhodamine-conjugated phalloidin and ER-Tracker Blue-White DPX, respectively. CLSM observations revealed that there were no obvious differences in cytoskeleton structure between cells that had internalized the MGs and control cells (Fig. 5a–f). Moreover, the structure and distribution of the ER were not visibly affected either (Fig. 5g–i). This insignificant influence was probably due to the relatively small cellular uptake number of the MGs[32] and the slight change in intracellular homeostasis.[40,41]

In biomedical applications, many synthesized micro/nano-materials have exhibited non-negligible immunogenicity with different mechanisms.[42–44] Hence, it is essential to examine the influence of materials on inflammation. In this regard, the effects of the MGs on mononuclear macrophages were investigated by co-incubation with RAW264.7 cells *in vitro*. Fig. 6a and b show that the cellular uptake behavior of RAW264.7 cells was similar to that of HepG2 and HepLi cells. Under the same conditions, more CSEG-*g*-Chol MGs were internalized. After co-incubation for 12 h, the percentages of RAW264.7 cells that had internalized MGs had reached their maximum values, which were 21.0% and 10.5% for CSEG-*g*-Chol MGs and ADEG-*g*-Chol MGs, respectively (Fig. 6a). Both the cellular uptake ratios and the cellular uptake numbers were relatively low in comparison with other types of particles.[45,46]
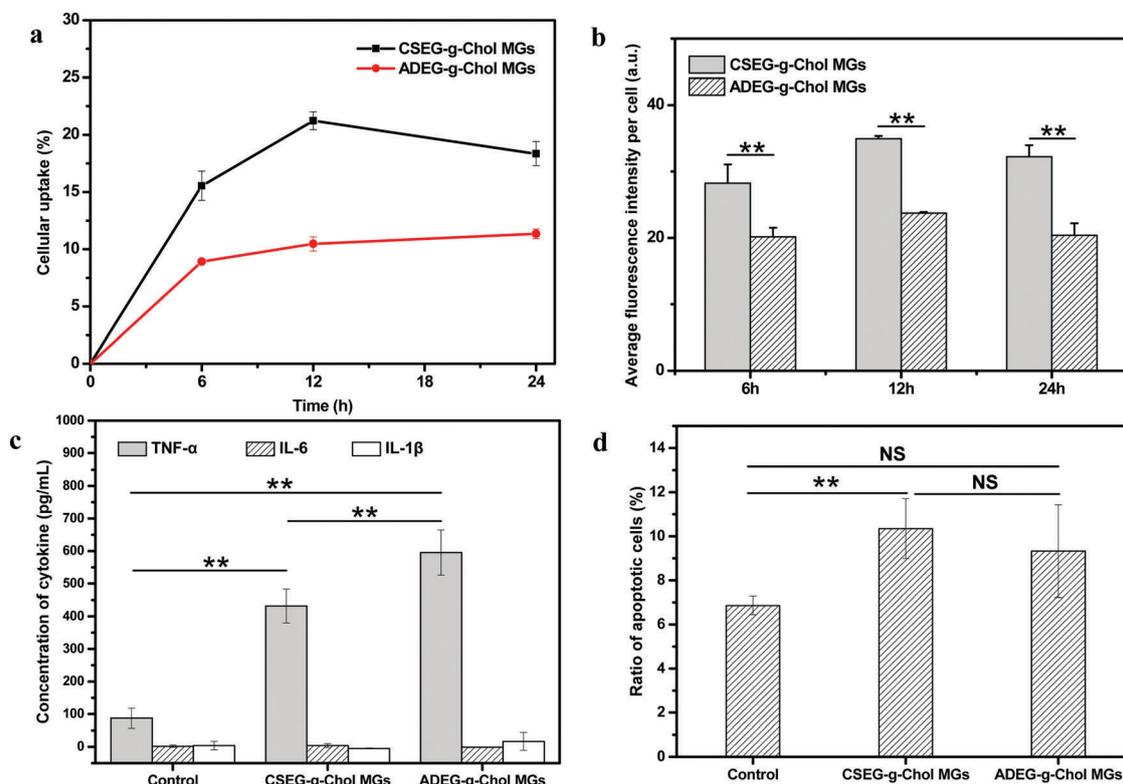

Fig. 6 Flow cytometry results showing the cellular uptake performance of RAW264.7 cells: the ratio of cells that internalized MGs as a function of the incubation time (a) and the cellular uptake amount of CSEG-*g*-Chol MGs and ADEG-*g*-Chol MGs (b) after co-incubation for a designated time at a particle : cell ratio of 15 : 1. (c) Secretion of TNF-α, IL-6 and IL-1β by RAW264.7 cells incubated with CSEG-*g*-Chol MGs and ADEG-*g*-Chol MGs, respectively, at a particle : cell ratio of 15 : 1 for 24 h. (d) Ratio of apoptotic RAW264.7 cells after being incubated with CSEG-*g*-Chol MGs and ADEG-*g*-Chol MGs at a particle : cell ratio of 15 : 1 for 24 h. The ratios of apoptotic cells were determined by flow cytometry after the cells were stained with annexin V-FITC/PI. Data are expressed as the mean ± SD, $n = 3$, *$p < 0.05$, **$p < 0.01$. NS indicates no significant difference at a level of $p < 0.05$.

The secretion of tumor necrosis factors (*e.g.*, TNF-α) and interleukins (*e.g.*, IL-6 and IL-1β) can be regarded as a typical activation signal for macrophages.[47,48] These factors are largely involved in inflammatory and immune responses. Therefore, the concentrations of these three cytokines in the culture supernatant were determined after RAW264.7 cells were co-incubated with CSEG-*g*-Chol MGs and ADEG-*g*-Chol MGs, respectively, for 24 h. Fig. 6c shows that the secretion of TNF-α in the MGs groups was several times higher than in the control group, and the value for the ADEG-*g*-Chol MGs group was the highest (1.3 times the value for the CSEG-*g*-Chol group). The secretion of IL-6 and IL-1β was at a very low level, and there were no significant differences between any of the groups. The secretion of TNF-α is a typical sign of the activation of macrophages, and its level can generally be associated with the degree of immune responses.[49] Therefore, the MGs can induce inflammatory responses, and the ADEG-*g*-Chol MGs have a more obvious effect.

Furthermore, the relative viability (Fig. S19, ESI†) and apoptosis rate (Fig. 6d) of RAW264.7 cells were measured. The relative cell viability in the ADEG-*g*-Chol group (75–82%) was lower than that in the CSEG-*g*-Chol group (90–97%) at the same particle : cell ratio (ESI,† Fig. S19). However, similar degrees of cell apoptosis were induced in the CSEG-*g*-Chol group (10.3%) and the ADEG-*g*-Chol group (9.3%), which were both higher than that in the control group (6.9%) (Fig. 6d). These results imply that uptake of the MGs impaired cell viability to some extent and obviously caused more apoptosis of RAW264.7 cells, which may intrinsically be related to the higher secretion of TNF-α.

Conclusions

We have put forward a novel and general strategy for the preparation of uniform microgels with synthesized polymers using a templating-crosslinking method. The CSEG-*g*-Chol MGs that were obtained underwent a reduction-responsive structural transformation, which was induced by the cleavage of disulfide bonds in the presence of reductants such as GSH and DTT. As a result, nanospikes protruded from the surface of the CSEG-*g*-Chol MGs to give a novel kind of micro/nanocomposite structures. When CSEG-*g*-Chol MGs were internalized by cells, reduction-responsive self-assembly and the protrusion of nanospikes occurred in the cell milieu *in situ* owing to the presence of GSH. No obvious influence on the cytoskeleton and endoplasmic reticulum was observed *via* light microscopy. However, the MGs exhibited a certain extent of cytotoxicity depending on the co-incubation concentration and stimulated the secretion of TNF-α. By this proof-of-concept study, we have successfully demonstrated for the first time that well-defined self-assembled nano/microstructures can be obtained by intracellular stimuli-responsive self-assembly. By using stimuli-responsive microgels with relatively large sizes as a platform, self-assembled nanospikes on their surface can easily be observed in cells, which is still a challenging task. This work may serve as a paradigm for the study of intracellular and *in vivo* self-assembly and may also provide important insights for the investigation of biological self-assembly.

Future work may involve the further study of intracellular self-assembly in the context of interactions with cells and biomedical applications.

Conflicts of interest

There are no conflicts to declare.

Acknowledgements

References

1 Y. Zhao, F. Sakai, L. Su, Y. J. Liu, K. C. Wei, G. S. Chen and M. Jiang, *Adv. Mater.*, 2013, **25**, 5215–5256.

2 G. M. Whitesides and B. Grzybowski, *Science*, 2002, **295**, 2418–2421.

3 G. A. Ozin, K. Hou, B. V. Lotsch, L. Cademartiri, D. P. Puzzo, F. Scotognella, A. Ghadimi and J. Thomson, *Mater. Today*, 2009, **12**, 12–23.

4 M. A. C. Stuart, W. T. S. Huck, J. Genzer, M. Muller, C. Ober, M. Stamm, G. B. Sukhorukov, I. Szleifer, V. V. Tsukruk, M. Urban, F. Winnik, S. Zauscher, I. Luzinov and S. Minko, *Nat. Mater.*, 2010, **9**, 101–113.

5 E. G. Kelley, J. N. L. Albert, M. O. Sullivan and T. H. Epps, *Chem. Soc. Rev.*, 2013, **42**, 7057–7071.

6 W. B. Zhang and C. Y. Gao, *J. Mater. Chem. A*, 2017, 5.

7 S. Mura, J. Nicolas and P. Couvreur, *Nat. Mater.*, 2013, **12**, 991–1003.

8 Y. L. Colson and M. W. Grinstaff, *Adv. Mater.*, 2012, **24**, 3878–3886.

9 W. B. Zhang, H. Y. Li, Y. Qin and C. Y. Gao, *Mater. Horiz.*, 2017, **4**, 1135–1144.

10 G. L. Liang, H. J. Ren and J. H. Rao, *Nat. Chem.*, 2010, **2**, 54–60.

11 J. Zhou, X. Du, J. Li, N. Yamagata and B. Xu, *J. Am. Chem. Soc.*, 2015, **137**, 10040–10043.

12 Y. Yuan, L. Wang, W. Du, Z. L. Ding, J. Zhang, T. Han, L. N. An, H. F. Zhang and G. L. Liang, *Angew. Chem., Int. Ed.*, 2015, **54**, 9700–9704.

13 Y. Gao, J. F. Shi, D. Yuan and B. Xu, *Nat. Commun.*, 2012, **3**, 1033.

14 D. Zhang, G. B. Qi, Y. X. Zhao, S. L. Qiao, C. Yang and H. Wang, *Adv. Mater.*, 2015, **27**, 6125–6130.

15 X. Huang, S. R. Raghavan, P. Terech and R. G. Weiss, *J. Am. Chem. Soc.*, 2006, **128**, 15341–15352.

16 S. Majumdar, A. Hajduczki, R. Vithayathil, T. J. Olsen, R. M. Spitler, A. S. Mendez, T. D. Thompson and G. A. Weiss, *J. Am. Chem. Soc.*, 2011, **133**, 9855–9862.

17 Y. V. Zastavker, N. Asherie, A. Lomakin, J. Pande, J. M. Donovan, J. M. Schnur and G. B. Benedek, *Proc. Natl. Acad. Sci. U. S. A.*, 1999, **96**, 7883–7887.

18 A. Radhakrishnan, J. L. Goldstein, J. G. McDonald and M. S. Brown, *Cell Metab.*, 2008, **8**, 512–521.

19 H. Wang, Z. Feng, D. Wu, K. J. Fritzsching, M. Rigney, J. Zhou, Y. Jiang, K. Schmidt-Rohr and B. Xu, *J. Am. Chem. Soc.*, 2016, **138**, 10758–10761.

20 K. Nagahama, Y. Ueda, T. Ouchi and Y. Ohya, *Biomacromolecules*, 2007, **8**, 3938–3943.

21 P. Pescador, N. Brodersen, H. A. Scheidt, M. Loew, G. Holland, N. Bannert, J. Liebscher, A. Herrmann, D. Huster and A. Arbuzova, *Chem. Commun.*, 2010, **46**, 5358–5360.

22 N. Morimoto, S. Hirano, H. Takahashi, S. Loethen, D. H. Thompson and K. Akiyoshi, *Biomacromolecules*, 2013, **14**, 56–63.

23 Y. L. Yang, Q. L. Chan, X. J. Ma, K. Deng, Y. T. Shen, X. Z. Feng and C. Wang, *Angew. Chem., Int. Ed.*, 2006, **45**, 6889–6893.

24 J. C. Lim and D. W. Chung, *J. Appl. Polym. Sci.*, 2012, **125**, 888–895.

25 A. Gong, X. H. Ma, L. C. Xiang, W. Z. Ren, Z. Y. Shen and A. G. Wu, *Colloids Surf., B*, 2014, **116**, 561–567.

26 W. Wei, L. Y. Wang, L. Yuan, Q. Wei, X. D. Yang, Z. G. Su and G. H. Ma, *Adv. Funct. Mater.*, 2007, **17**, 3153–3158.

27 B. Stadler, R. Chandrawati, A. D. Price, S. F. Chong, K. Breheney, A. Postma, L. A. Connal, A. N. Zelikin and F. Caruso, *Angew. Chem., Int. Ed.*, 2009, **48**, 4359–4362.

28 K. Engberg, D. J. Waters, S. Kelmanovich, R. Parke-Houben, L. Hartmann, M. F. Toney and C. W. Frank, *Polymer*, 2016, **84**, 371–382.

29 M. L. Bushey, T. Q. Nguyen, W. Zhang, D. Horoszewski and C. Nuckolls, *Angew. Chem., Int. Ed.*, 2004, **43**, 5446–5453.

30 W. Pisula, M. Kastler, D. Wasserfallen, T. Pakula and K. Mullen, *J. Am. Chem. Soc.*, 2004, **126**, 8074–8075.

31 M. R. H. Krebs, C. E. MacPhee, A. F. Miller, I. E. Dunlop, C. M. Dobson and A. M. Donald, *Proc. Natl. Acad. Sci. U. S. A.*, 2004, **101**, 14420–14424.

32 B. Wang, Y. Y. Zhang, Z. W. Mao and C. Y. Gao, *Macromol. Biosci.*, 2012, **12**, 1534–1545.

33 Y. Y. Yuan, R. T. K. Kwok, G. X. Feng, J. Liang, J. L. Geng, B. Tang and B. Liu, *Chem. Commun.*, 2014, **50**, 295–297.

34 A. Meister, *J. Biol. Chem.*, 1988, **263**, 17205–17208.

35 H. S. Wang, W. Yu, W. B. Zhang and C. Y. Gao, *Macromol. Biosci.*, 2014, **14**, 1748–1754.

36 H. S. Wang, W. B. Zhang and C. Y. Gao, *Biomacromolecules*, 2015, **16**, 2276–2281.

37 D. A. Fletcher and R. D. Mullins, *Nature*, 2010, **463**, 485–492.

38 M. Michalak, *Semin. Cell Dev. Biol.*, 2010, **21**, 471.

39 X. Yang, H. Shao, W. Liu, W. Gu, X. Shu, Y. Mo, X. Chen, Q. Zhang and M. Jiang, *Toxicol. Lett.*, 2015, **234**, 40–49.

40 X. Yang, H. Shao, W. Liu, W. Gu, X. Shu, Y. Mo, X. Chen, Q. Zhang and M. Jiang, *Toxicol. Lett.*, 2015, **234**, 40–49.

41 L. Cole, D. Davies, G. J. Hyde and A. E. Ashford, *Fungal Genet. Biol.*, 2000, **29**, 95–106.

42 M. A. Dobrovolskaia, D. R. Germolec and J. L. Weaver, *Nat. Nanotechnol.*, 2009, **4**, 411–414.

43 M. A. Dobrovolskaia, M. Shurin and A. A. Shvedova, *Toxicol. Appl. Pharmacol.*, 2016, **299**, 78–89.

44 B. S. Zolnik, A. F. González-Fernández, N. Sadrieh and M. A. Dobrovolskaia, *Endocrinology*, 2010, **151**, 458–465.

45 X. Chen and C. Gao, *Colloids Surf., B*, 2017, **160**, 372–380.

46 Y. Zhang, Y. Xu, X. Xi, S. Shrestha, P. Jiang, W. Zhang and C. Gao, *J. Mater. Chem. B*, 2017, **5**, 3521–3530.

47 K. L. Spiller, R. R. Anfang, K. J. Spiller, J. Ng, K. R. Nakazawa, J. W. Daulton and G. Vunjak-Novakovic, *Biomaterials*, 2014, **35**, 4477–4488.

48 E. Giraudo, L. Primo, E. Audero, H. P. Gerber, P. Koolwijk, S. Soker, M. Klagsbrun, N. Ferrara and F. Bussolino, *J. Biol. Chem.*, 1998, **273**, 22128–22135.

49 H. Kikuchi, H. Yagi, H. Hasegawa, Y. Ishii, K. Okabayashi, M. Tsuruta, G. Hoshino, A. Takayanagi and Y. Kitagawa, *J. Surg. Res.*, 2014, **190**, 134–143.

This journal is © The Royal Society of Chemistry and the Chinese Chemical Society 2019

Mater. Chem. Front., 2019, **3**, 233–241 | 241